Eur. Phys. J. B **9**, 389–399 (1999)

THE EUROPEAN PHYSICAL JOURNAL B

EDP Sciences

Particle size effect of a.c. superconducting properties in $Tl_2Ca_1Ba_2Cu_2O_8$ compound

I. Kirschner[1,a], R. Laiho[2], A.C. Bódi[3], A.D. Caplin[4], E. Lähderanta[2], G. Zsolt[1], and I. Halász[5]

[1] Institute of Physics, Eötvös University, 1117 Budapest, Hungary
[2] Wihuri Physical Laboratory, University of Turku, 20014 Turku, Finland
[3] Institute of Experimental Physics, Kossuth University, 4001 Debrecen, Hungary
[4] Centre for High Temperature Superconductivity, Imperial College, SW7 2BZ London, Great Britain
[5] Central Research Institute of Chemistry, 1025 Budapest, Hungary

Received 10 October 1998

Abstract. Using a new starting material of $Ba_2Cu_3O_5$ and a three step heat treatment, single phase $Tl_2Ca_1Ba_2Cu_2O_8$ high-T_c superconducting samples have been prepared, possessing the onset- and critical temperatures $T_o = 114$ K and $T_c = 105$ K. The morphology dependent value of H_{c1} is 17 Oe, 8 Oe and 5 Oe at 77 K in the case of bulk, crushed and powdered materials, respectively. The a.c. susceptibility, r.f. susceptibility and microwave absorption properties show a significant dependence on the particle size with a sharp change in the interval between 750 μm and 1200 μm. These experiments provide characteristic parameters for intergrain material (treated as 3D Josephson network) as $\lambda_J = 0.8$ mm, $H_{Jc} = 0.28$ Oe and $J_{Jc} = 2.2$ A/cm^2 at 77 K. The data are controlled by modulated microwave absorption measurements. The results obtained can be explained well both by the finite size junction model and cavity mode absorption model. The Josephson network is determined unambiguously by metallic S–N–S weak links.

PACS. 74.25.-q General properties; correlations between physical properties in normal and superconducting states – 74.40.+k Fluctuations (noise, chaos, nonequilibrium superconductivity, localization, etc.) – 75.40.-s Critical-point effects, specific heats, short-range order

1 Introduction

As the early investigations of Tl-Ca-Ba-Cu-O high-T_c superconducting compounds showed [1,2], their structural, electrical, magnetic, thermal and pinning properties are substantionally affected by the preparation process used. According to high number of very different kinds of both earlier and later experiments [3–5] the superconducting characteristics of Tl-based compounds are strongly sensitive to the chemical quality and mixing ratios of the starting materials and to the heat treatment procedures. This is the reason why the critical temperature can vary in a wide interval even within a given nominal composition (see Tab. 1). Its differences may be looked for in Tl non-stoichiometry, in stacking defects appearing in the rock salt and perovskite units and in deviations of local and global distribution of the given material composition or phase, caused by preparation details. The starting compounds (oxides, cuprates, nitrates) do not react in general to produce directly a single-phase superconductor of the composition predictable in advance. Besides the basic (1, 1, 2, 2), (1, 2, 2, 3), (1, 3, 2, 4), (2, 0, 2, 1), (2, 1, 2, 2) and (2, 2, 2, 3) phases, other non-stoichiometric modifications can also be formed, depending on fine details of the preparation, which lead sometimes to temporarily changing [6] unstable samples.

Since the behavior of the superconductivity of powdered materials differs significantly from that of the same type of bulk specimens [7–9], it seems to be reasonable to study the dependence of r.f. magnetic susceptibility and microwave absorption on the particle size, expecting further useful information from points of view of fundamental research and applications, too.

2 Sample preparation and characterization

The specimens were composed from a non-conventional type of barium cuprate $Ba_2Cu_3O_5$ [10,11] by adding $TlNO_3$ and CaO to it in an appropriate amount in order to get samples abundant in the $Tl_2Ca_1Ba_2Cu_2O_8$ phase.

The double-metal $Ba_2Cu_3O_5$ oxide was prepared by solid state reaction of analytical grade Merck chemicals of $Ba(NO_3)_2$ and CuO, using their mixture in the molar ratio of 1:1.5. This mixture was fired in air at 940 °C for 5 h, followed by a slow cooling to room temperature. The product obtained can be identified as a new barium cuprate of the composition $Ba_2Cu_3O_5$. Its X-ray diffraction pattern

[a] e-mail: ikirschner@ludens.elte.hu

Table 1. Structural properties and critical temperatures of different Tl-Ca-Ba-Cu-O compounds. (The actual measured T_c depends on the quality and mixtures of the phases of the given specimen.)

Phase	Structure of unit cell	Lattice constants a and c (Å)	Critical temperature (K)
(1, 1, 2, 2) $Tl_1Ca_1Ba_2Cu_2O_7$	prim. tetragonal	3.84 & 12.63	65–85
(1, 2, 2, 3) $Tl_1Ca_2Ba_2Cu_3O_9$	prim. tetragonal	3.84 & 15.87	100–110
(1, 3, 2, 4) $Tl_1Ca_3Ba_2Cu_4O_{11}$	prim. tetragonal	3.85 & 19.12	110–120
(2, 0, 2, 1) $Tl_2Ba_2Cu_1O_6$	b.c. tetragonal	3.86 & 23.23	20–80
(2, 1, 2, 2) $Tl_2Ca_1Ba_2Cu_2O_8$	b.c. tetragonal	3.86 & 29.32	95–105
(2, 2, 2, 3) $Tl_2Ca_2Ba_2Cu_3O_{10}$	b.c. tetragonal	3.85 & 35.88	115–125

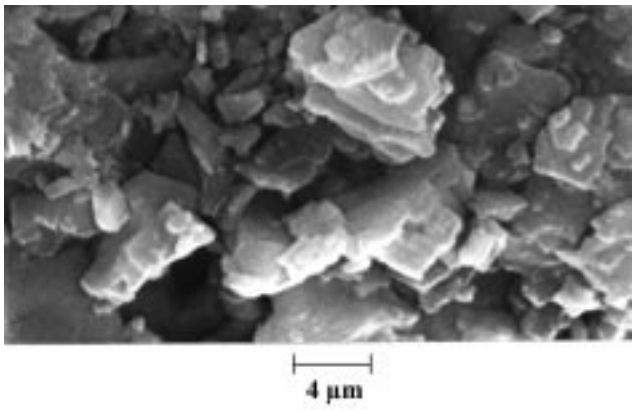

Fig. 1. Typical scanning electron micrographs of the samples.

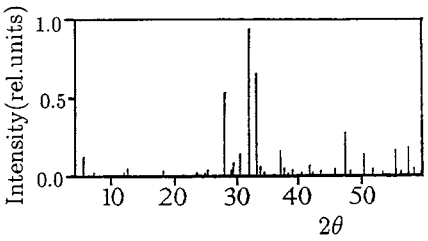

Fig. 2. X-ray diffractogram, showing the composition of the specimens.

can well be indexed in tetragonal structure with lattice parameters $a = 9.16$ Å and $c = 12.96$ Å. The favorable experiences [12] got during the application of $Ba_2Cu_3O_5$ in the preparation of Y-based compounds prompted us to employ it as a starting material of Tl-Ca-Ba-Cu-O superconductors.

The applied, rather complicated, three-step thermal annealing has served to reach a single-phase or quasi-single-phase material. After grinding and mixing the above mentioned starting compounds, they were at first pre-heated at 400 °C in air for 0.5 h and then cooled to room temperature with a rate of 100 °C/h. The first high temperature solid state reaction was realized by a heat treatment at 800 °C in air for 0.5 h, followed by a slow cooling of 10 °C/min to the ambient temperature. The product obtained was ground and mixed again and pressed into blocks by pressure of 5 MPa. These pellets were submitted to sintering at 900 °C in air for 10 min to finish fully the reactions, then cooled down to 800 °C during 10 min, and this step was continued with a quick cooling to room temperature in the course of a 5 min time range. (After this process, the optimum or nearly optimum doping can be attained by reannealing of the samples alternatively in oxygen and argon).

The quality of the specimens was characterized by scanning electron microscopy, X-ray diffractography, resistivity, a.c. susceptibility and d.c. magnetization measurements, moreover by detecting the hysteresis loops in low magnetic fields.

As the SEM photos demonstrate in Figure 1, the samples have a homogeneous microstructure of low porosity, where some part of microcrystals are rounded. In some places partially melted, glass-like small domains can also be observed, existing probably due to the quick final cooling. This investigation shows a random grain size distribution with linear dimensions of 2−8 μm.

In order to estimate the share-rate of different components of sample's material the relative intensity of X-ray diffraction lines (see Fig. 2) was employed. On this basis, the well-crystallized specimens can be considered as single-phase ones from the point of view of superconductivity. They possess (2, 1, 2, 2) phase up to 77–80% as pointed out by high intensity lines at $2\Theta = 6.03°$ and 27.77°, having closely ideal tetragonal unit cells

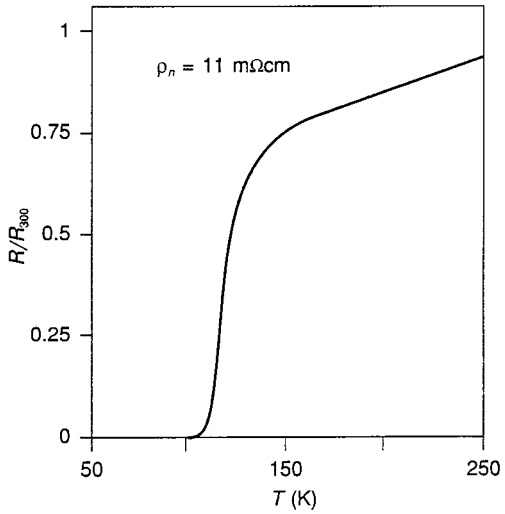

Fig. 3. Low specific normal resistivity and the sharp drop of the function of the resistance on the temperature demonstrate the good superconducting quality of investigated specimens.

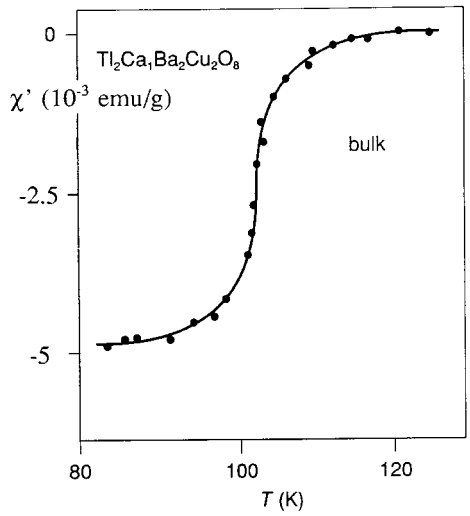

Fig. 4. Real part of a.c. susceptibility of the bulk material.

with lattice parameters of $a = 3.86$ Å and $c = 29.34$ Å. This material content is accompanied by a low quantity of some residual $Ba_2Cu_3O_5$. The peak at $2\Theta = 7.60°$ hints at the presence of (2, 0, 2, 1) phase in quantity less than 1–2%. The existence of low quantity CuO and Cu_2O is indicated by weak lines at $2\Theta = 35.49°$, $35.57°$, $38.77°$ moreover $36.50°$ and $42.34°$, respectively. As an interesting consequence of the heat treatment procedure mentioned above, some CaO compound can be detected in the samples, as is demonstrated by the line at $2\Theta = 37.45°$. Diffraction lines at $2\Theta = 37.51°$, $41.31°$ and $46.65°$ are not identified.

Powder X-ray diffraction patterns were taken for the intermediate products, too, obtained after the 800 °C heat treatment. This shows that starting materials are already almost fully reacted at the temperatures of about 800 °C. The observed character of the reactions is in contradiction with certain previous experience [13], by which temperatures above 900 °C are indispensable for solid state reactions while preparing Tl-Ca-Ba-Cu-O superconductors.

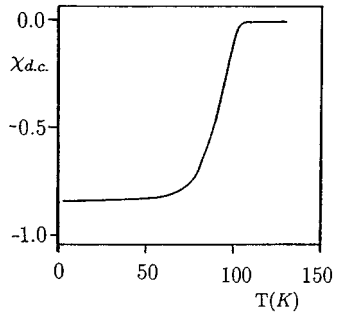

Fig. 5. The d.c. susceptibility hints at the single-phase character of samples.

Analyzing all of the experiences attained during our prolonged research in the field of Tl-Ca-Ba-Cu-O superconductors, it can be concluded that in the creation of (2, 1, 2, 2) phase not only the volatility of the Tl-ions, but the building in of the Ca-ions plays also a fundamental role. This statement is confirmed on the one hand, by the majority character of the formation of (2, 1, 2, 2), the existence of the (2, 0, 2, 1), the permanent appearance of CaO and on the other hand, by the minority character of the occurrence of the (2, 2, 2, 3) phase and the presence of the single Tl-O plane containing (1, 1, 2, 2) and (1, 2, 2, 3) phases only in traces. All these arguments indicate that the development of the (2, 1, 2, 2) phase is the most probable both from the points of view of thermodynamical aspect and optimum chemical coordination, under the given initial circumstances.

In order to get reliable information on superconducting properties of the bulk samples, the temperature dependence of their resistance was measured by conventional four-probe method under isothermic conditions. The specimens have low room temperature specific resistivity, metallic behavior in the whole temperature interval and relatively narrow superconducting transitional range. As is seen in Figure 3, this measurement provides values for the onset and zero resistivity critical temperature as $T_o = 114$ K and $T_c = 105$ K.

The normal-superconducting transition was also followed by the temperature dependence of the real component χ' of the complex a.c. susceptibility χ (see Fig. 4). The measurements were performed by a double-coil system at the frequency of 10 kHz, reflecting the high superconducting material content and a.c. magnetic onset temperature $T_o^m = 118$ K, that may hint either at the presence of very small amount of discretely distributed (2, 2, 2, 3) phase of higher T_c, or at some locally occurring mixed unit cells of the intergrowth of different phases of higher and lower T_c, or by chance at small, local material domains in certain places, containing stacking faults along the *c*-axis.

Temperature dependence of d.c. magnetization was measured by a SQUID magnetometer. Its results reflect the superconducting quality and the phase structure of the specimens. The experimental data obtained for d.c. susceptibility (Fig. 5) demonstrate the single-phase

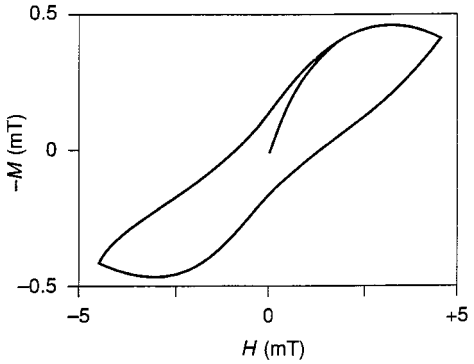

Fig. 6. Low field hysteresis measurement provides value for lower critical magnetic field H_{c1} for bulk material as 1.8 mT.

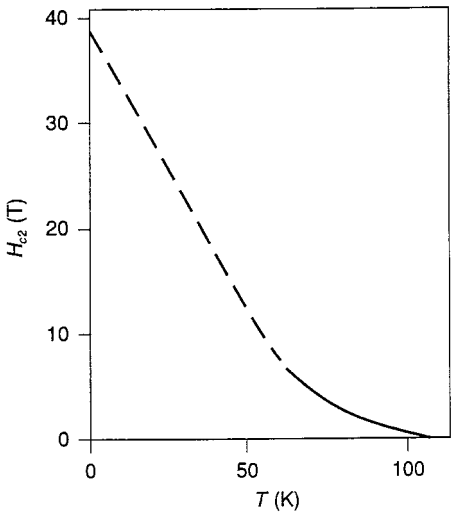

Fig. 7. The linear continuation of the measured high temperature magnitudes of the upper critical magnetic field leads to its zero temperature value of $H_{c2}(0) = 39$ T.

superconducting character of the samples, in which the temperature of the drastic diamagnetic transition T_d coincides with the electrical critical temperature, having values of 104–105 K.

The lower critical magnetic field H_{c1} of the specimens was determined by detecting magnetic hysteresis loops taken between −5 mT and +5 mT at liquid nitrogen temperature by using a vibrating sample magnetometer. As Figure 6 demonstrates, this measurement provides the value of $H_{c1}(77\ \mathrm{K}) = 1.7$ mT. Following an earlier supposition on the nearly linear character of H_{c1}–T curve [14,15] of Tl-Ca-Ba-Cu-O compounds, it leads to $H_{c1}(0) = 6.4$ mT.

At the same time, the irreversibility of the low field magnetization process can also be characterized by this experiment, giving the trapped flux as the share-rate of the sweeping interval of the applied magnetic field. Its value is 9–10%, reflecting the homogeneous microstructure of the samples.

Thermodynamic critical magnetic field $H_c(0)$ can be estimated on the basis of Mühlschlegel formula [16]

$$H_c(0) = \left(\frac{2\pi}{V_m}\right)^{1/2} \gamma(0) T_c, \tag{1}$$

derived from the condensation energy in the framework of the BCS-theory in the form of a similarity law. It results in a magnitude of 340 mT. (Here V_m is the molar volume and γ is the electronic specific heat coefficient, having generally the experimental values [17] of 15–16 mJ/mol grad^2).

Investigation of the resistivity in a changing external magnetic field (in our case up to 7 T) at different temperatures can serve to estimate the magnitude of the upper critical magnetic field $H_{c2}(0)$ by the application of the appropriate relations of GLAG-theory [18–20] for impurity superconductors of low mean free path

$$H_{c2}(0) = 2.6\,\gamma(0)\,T_c\,\rho_n, \tag{2}$$

moreover

$$H_{c2}(t) = (1.77 - 2.2t^2 + 0.5t^4 - 0.07t^6)\kappa(T_c)H_c(0), \tag{3}$$

the Bardeen [21] - Ginzburg [22] equation

$$H_{c2}(t) = 2\sqrt{2}\kappa(T_c)H_c(0)\frac{1-t^2}{1+t^2} \tag{4}$$

and the Helfand-Werthamer-Hohenberg [23] dirty limit formula

$$H_{c2}(0) = 0.69\,T_c \left(\frac{\mathrm{d}H_{c2}(T)}{\mathrm{d}T}\right)_{T_c}, \tag{5}$$

that attempts to deduce the zero-temperature values of the curve H_{c2}–T from its shape at high temperatures and low magnetic fields. (In these formulae ρ_n is the specific resistivity of the normal state before superconducting transition, $t = T/T_c$, κ is the Ginzburg-Landau parameter and H_c is the thermodynamic critical magnetic field). Since the experimental shape of the H_{c2}–T curve in the attained measuring interval deviates significantly from these relations, the linear approximation seems to be the most plausible way to estimate the scale of H_{c2} at low temperatures. As Figure 7 shows, this procedure leads to the value of $H_{c2}(0) = 39$ T for our samples.

3 Measurements and results

The propagation of any physical (*e.g.* electrical or thermal) effect or the motion of any "particle" (*e.g.* magnetic vortex) in high-T_c superconductors is determined by their granular nature. In these materials the grains are coupled to each other by Josephson links (or by proximity effect) [24–26] and the existence of intragranular junctions was observed even in single crystals, too [27,28] which represent a coupling across thin defect planes or boundaries inside a given grain. In this meaning the intergrain and intragrain properties of these samples can be distinguished

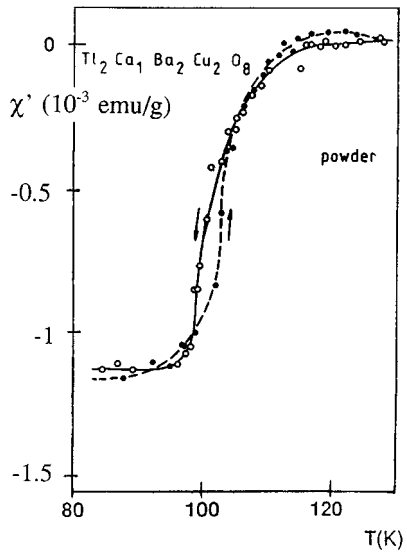

Fig. 8. The shape of the function of the real part of complex a.c. susceptibility the powder on the temperature demonstrates the same chemical composition, physical structure and so characteristic temperatures as the bulk material, but shows less superconducting content.

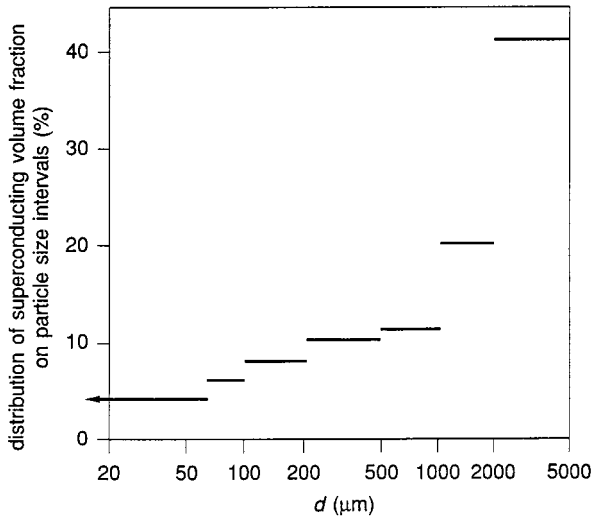

Fig. 9. Distribution of the superconducting volume fraction on particle size intervals. (The sharp increase begins at the particle size of ~ 0.8 mm.)

and even separated by experimental methods [29–31]. On the other hand, the high frequency and microwave measurements can be applied to study the particle size effects in crushed, powdered and fine powder based specimens [32–35].

The originally bulk samples were crushed into powder of various particle sizes and filtered through successive sieves. By this method seven different powder specimens were separated in the particle size interval of $2 \leq d \leq 5000\,\mu$m. At first, the normal-superconducting (N–S) and superconducting-normal (S–N) transitions were detected by the measurement of $\chi' - T$ function during cooling and heating processes between room- and liquid nitrogen temperatures. The functions $\chi' - T$, moreover $\chi' - H$ and that of the imaginary part of χ, *i.e.* $\chi'' - H$ below T_c were measured by using a commercial R-L-C meter and based on an r.f. oscillator which was working at the frequency of 2 MHz, having a usual pick-up coil of inductivity of $L = 15\,\mu$H. The measurements were based on the comparison of the values obtained without and with samples. The change of the temperature and magnetic field gave rise not only to the variation of χ of the samples and the resonance frequency of the R-L-C oscillator, but that of the quality factor of the resonant circuit, too. The former were measured by a high resolution (5×10^{-9}) frequency counter, while the latter *via* the bandwidth of the resonance curve. (It must be noted that no correction was applied for demagnetization or porosity.) The temperature was regulated by changing distance of the sample holder coil to liquid nitrogen surface and measured by Fe-constantan thermocouples. All χ'–H and χ''–H experiments were realized at liquid nitrogen temperature. During the direct and field modulated microwave absorption measurements the samples (having exactly 20 mg mass) were placed in a quartz dewar and introduced into the cavity of an X-band (9 GHz) ESR spectrometer at the maximum value of the microwave magnetic field. The residual d.c. magnetic field of the equipment's electromagnet was always externally compensated. In these experiments, strictly identical operating conditions of the spectrometer were used to ensure unambiguous comparison of the observed spectra. The amplitudes of the direct microwave absorption signals were compared at $H = 60$ Oe.

Since the shape and characteristic parameters of functions $\chi' - T$ are very sensitive to the chemical composition and physical state of the specimens, the comparison of these curves, concerning bulk, crushed and powdered samples can demonstrate their similar or deviating character. As the results of the measurements carried out on a ground specimen in Figure 8 show, the slope and characteristic temperatures did not change during the grinding, proving the identical chemical composition and physical structure of bulk and crushed materials. The observed drastic decrease of the global superconducting content, however, shows that the particles are well separated by grinding and the ground sample behaves as a set of independent particles.

On the basis of $\chi' - T$ measurements, the share-rates of the full superconducting volume fraction is determined to be attributed to different ranges of the particle size d. This ratio increases slightly at first with particle size in the interval of $2\,\mu$m$-750\,\mu$m and then has a sharp increase above it (see Tab. 2 and Fig. 9). It means that the grains of $d \geq 1$ mm establish coherent domains, which begin to behave as bulk material. It manifests itself even more strongly, if the normalized superconducting volume fraction, referring to 1% of the particle size ranges is calculated, as is listed in Table 2, too. This is the weight

Table 2. Particle size distribution, dependence of the share-rate of the total superconducting volume fraction on particle size intervals and the superconducting volume fraction related to 1% of different particle size ranges (treated as a weight factor).

Particle size intervals	Particle size distribution	Superconducting volume fraction distribution in different size intervals	Superconducting volume fraction referring to 1% of particle size intervals (*i.e.* weight factor)
$2\,\mu\text{m} < d < 63\,\mu\text{m}$	12%	4%	0.33%
$63\,\mu\text{m} < d < 100\,\mu\text{m}$	20%	6%	0.30%
$100\,\mu\text{m} < d < 200\,\mu\text{m}$	23%	8%	0.35%
$200\,\mu\text{m} < d < 500\,\mu\text{m}$	24%	10%	0.42%
$500\,\mu\text{m} < d < 1000\,\mu\text{m}$	12%	11%	0.92%
$1000\,\mu\text{m} < d < 2000\,\mu\text{m}$	3%	20%	6.67%
$2000\,\mu\text{m} < d < 5000\,\mu\text{m}$	6%	41%	6.83%

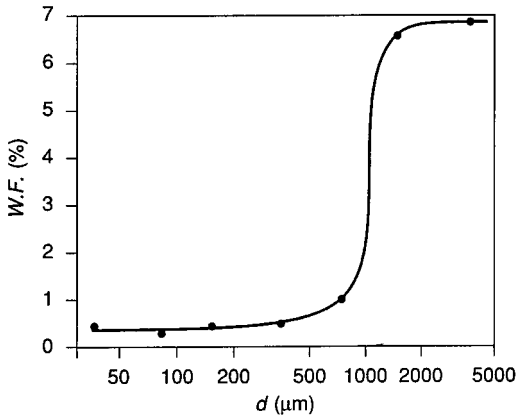

Fig. 10. Dependence of the superconducting volume fraction on the particle size, concerning 1% of different particle size intervals. This is explained as a weight factor W.F., showing the role of different particle size ranges in possessing the superconductivity.

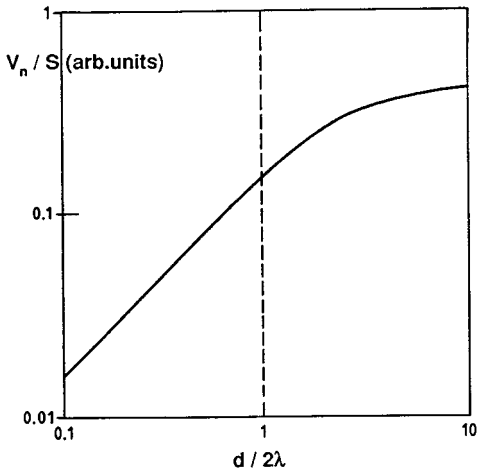

Fig. 11. Dependence of the ratio of V_n/S on the ratio of $d/2\lambda$ in a powdered sample, where V_n is the normal volume fraction, S is the total surface area, d is the particle size and λ is the London penetration depth.

factor W.F., that shows the role of particle size intervals in the development of superconducting state, as is demonstrated in Figure 10, by putting the W.F. points in the middle of each particle size range.

As a summary of these observations, a monotonous size effect can be stated for $Tl_2Ca_1Ba_2Cu_2O_8$ superconductor until about $1000\,\mu$m, which is followed by a transitional region into bulk behavior. This statement is confirmed by representing the function of the ratio of normal volume fraction V_n and total surface area S of powder samples under measurement *versus* $d/2\lambda$, where λ is the penetration depth (Fig. 11). As is seen, the curve shows a linear increase when $d \leq 2\lambda$ and tends to a saturation character well above this value. Supposing that the geometry of particles is mostly comparable to spheres, the shape of this curve can be described by the relations [31,35]

$$\frac{V_\text{n}}{S} \approx \frac{d}{2\pi}, \quad \text{if} \quad d \leq 2\lambda \tag{6}$$

and

$$\frac{V_\text{n}}{S} \approx \frac{3\lambda}{\pi}\left[1 - \frac{2\lambda}{d} - \frac{1}{3}\left(\frac{2\lambda}{d}\right)^2\right], \quad \text{if} \quad d \geq 2\lambda. \tag{6'}$$

It is worth to mention that the investigation analyzed above leads to very similar value of the linear dimensions of the coherent domains, as it was obtained in an earlier work when the existence of these domains was directly detected in $Y_1Ba_2Cu_3O_{7-\delta}$ specimens by a thermally non-equilibrium measuring method [36]. In the case of Y-samples investigated, the average value of domain's linear dimensions was given experimentally as 2.1 mm, while the present research provides this magnitude in the order of 1 mm for the Tl-specimens in question.

The dependence of the real part χ' and the imaginary part χ'' of χ on the external magnetic field were determined by an r.f. resonance method at $T = 77$ K.

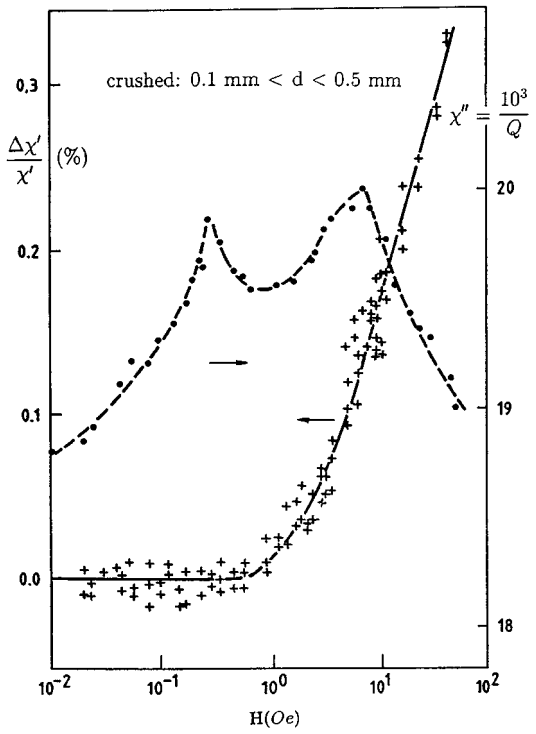

Fig. 12. Magnetic field dependence of the relative change of the real part χ' and that of the imaginary part χ'' of the r.f. susceptibility χ at $T = 77$ K.

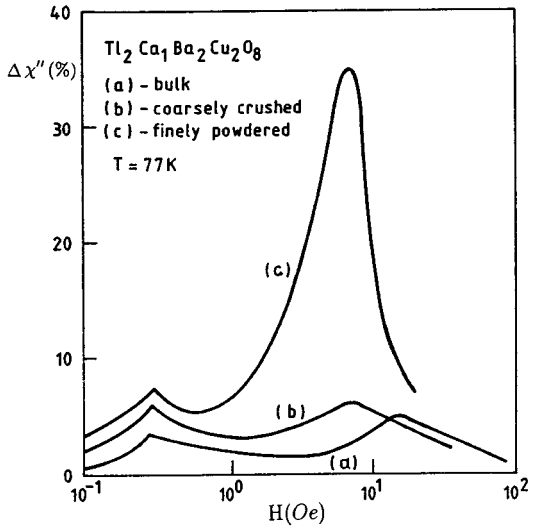

Fig. 13. Dependence of $\Delta\chi''$ on the magnetic field H of the bulk ($2\times2\times8\,\mathrm{mm}^3$), crushed ($0.1 < d < 0.5$ mm) and powdered ($d < 63\,\mu$m) specimens.

They demonstrate a two-stage transition between normal-superconducting or superconducting-normal state (see Fig. 12). Comparing the results obtained to each other belonging to the bulk ($2 \times 2 \times 8$ mm), coarsely crushed ($0.1\,\mathrm{mm} \le d \le 0.5\,\mathrm{mm}$) and finely powdered ($2\,\mu\mathrm{m} \le d \le 63\,\mu$m) samples (Fig. 13), the physical background of the characteristics measured can be drawn up, as follows:

1) At the fields low enough, when the energy of Josephson coupling surpasses the thermal fluctuation, both the weak links and the grains are still superconducting. Thus the initial part of $\Delta\chi'(H)/\chi'(H)$ is nearly linear and corresponds to the perfect diamagnetism. The external magnetic field is shielded by circulating supercurrents, flowing in the actual penetration depth to prevent the field to penetrate deeply into bulk, crushed or powdered specimens.
2) The location of the low field peaks of the $\Delta\chi''-H$ curve is independent of the particle size. They are formed due to the presence of intergrain junctions, which are able to carry supercurrent until the magnetic field, corresponding to the position of the first peaks on the H axis. This is the intergrain critical field $H_{\mathrm{ig}}(77\,\mathrm{K}) = 0.28$ Oe, which leads to its zero-temperature value as $H_{\mathrm{ig}}(0) = 0.61$ Oe or 1.1 Oe according to the quadratic or to the linear temperature dependence, respectively. Due to this reason, the r.f. susceptibility measurements can be evaluated to represent well the intergrain behavior of specimens, distinguishing the value of H_{ig} by the first peak on the absorption curve.
   The small increase in the height of the low field peak concerning crushed and powdered samples reflects probably the presence of a weak residual intragrain signal at the position of the intergrain peaks.
3) When H is increased further, the intergrain currents decrease, resulting in a reduction in the screening, moreover an increasing $\chi'(H)$ and a decreasing $\chi''(H)$. At the values of 0.7 Oe for powdered, 1.1 Oe for crushed and 3.8 for bulk specimens, the intragrain currents begin to become dominant and both $\chi'(H)$ and $\chi''(H)$ will increase.
4) If the field intensity is high enough to penetrate deeply into the grains, the r.f. hysteresis loss $\chi''(H)$ has a second maximum, the position of which on the H-axis depends strongly on the morphology of samples, having values of 5 Oe for powdered, 8 Oe for crushed and 17 Oe for bulk materials. These magnitudes describe directly the global-macroscopic granular nature of $Tl_2Ca_1Ba_2Cu_2O_8$ superconductors, representing their lower critical magnetic field H_{c1}. It includes together the sample's intergranular and intragranular properties and its deviating values reflect unambiguously again the particle size effect. The magnitude obtained from r.f. susceptibility investigation is in agreement with our earlier, low field hysteresis experiments (see Fig. 6) [37] carried out on this type of bulk samples, taking into account the value of H, when the magnetic moment $M(H)$ starts to deviate from its linear character.
5) Over the region of higher field peaks, the curves $\chi''-H$ decrease, because the increasing driving d.c. field onto that the r.f. field is superposed produces a continuously decreasing ratio of $H_{\mathrm{r.f.}}/H_{\mathrm{d.c.}}$ and together with this reducing hysteresis loops and r.f. losses.

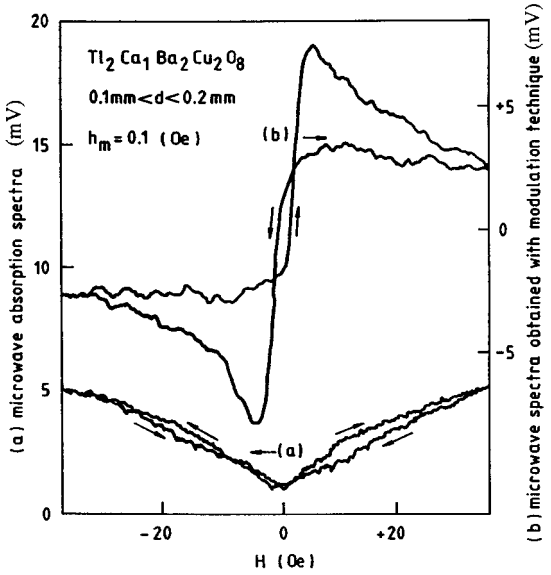

Fig. 14. Direct and modulated with $h_{\mathrm{m}} = 0.1$ Oe (field derivative) microwave absorption as the function of an external magnetic field H in the sample of $0.1\,\mathrm{mm} < d < 0.2$ mm.

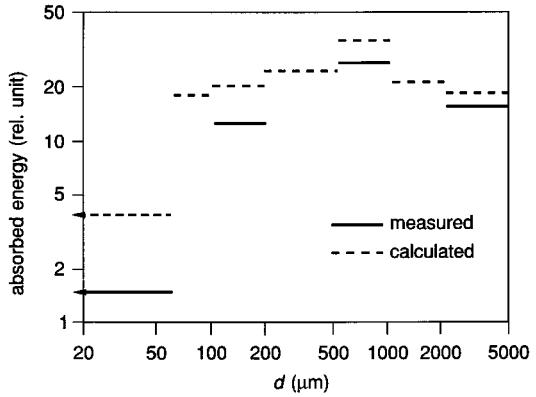

Fig. 15. Distribution of the microwave absorption on the particle size measured directly and calculated from the measured field derivative signals.

During the microwave measurements [38] all Tl-based specimens showed a hysteretic absorption spectrum (direct method) and a derivative signal with giant peaks (modulation method) at low external magnetic fields between −35 and +35 Oe. Typical spectra are demonstrated in Figure 14 at the temperature of 77 K. We suppose that the dissipation is caused by the damped oscillation of vortices under the effect of the forces, namely the microwave induced Lorentz-type moving force, the restoring force due to the flux pinning [39] and the damping short-range elasticity force originated from the intervortex interaction due to their non-equilibrium distribution [2]. The microwave absorption begins at very low magnetic field. Its value is determined by the thickness and density of intergranular and interparticle weak links in the samples. As the d.c. field is increased, more junctions will be involved in the process and the absorption increases monotonically. At a given value of d.c. field of about 5 Oe, where the maximum number of links participates in the interaction, the field derivative of the absorption shows a maximum, while the direct absorption spectra demonstrate a minimum near zero magnetic field. As the external magnetic field is increased further all the grains of the whole bulk matrix (or all the particles) up to the actual penetration depth will be affected by field and the superconductivity will disappear causing the saturation of the diamagnetic-type absorption. In the course of this process, the shape of the derivative of the microwave absorption signal reflect essentially the number of junctions, which are penetrated by different field intensities.

The energy absorbed can be calculated directly by numerical integration of the derivative curves and used as a characteristic parameter, when comparing the quality of different specimens.

A broad line (1 mT to 10 mT in Y-Ba-Cu-O samples) corresponding to an absorption minimum at zero magnetic field has been attributed directly to the damped motion of vortices with intergranular Josephson junctions [40,41]. A narrow line (0.01 mT to 0.1 mT) due to the absorption maximum has been observed in powdered materials [9] and explained by considering the particles as superconducting loops containing weak links.

The microwave absorption also demonstrates a significant particle size effect. At first it increases with increasing particle size until about 0.8 mm and after this maximum (see Fig. 15) decreases dramatically with further increasing particle size, when the possibility for the development of the above mentioned coherent domains is given.

As the experiments executed by the modulation method show, at this critical linear dimension range of the order of 1 mm not only the maximum of the absorption, but the sharp change of the line width of the derivative absorption spectra $\Delta H_{\mathrm{l.w.}}$ (see Fig. 16), too, indicates the distinguished role of this size in the establishing high-T_{c} superconductivity. This observation is supported by the representation of the peak height of the field derivative of the microwave absorption in the function of the particle size (Fig. 17), which also has a maximum in the vicinity of $d = 800\,\mu$m.

According to Figure 18, the microwave response, similarly to the r.f. one, is more intensive in ground samples, than in bulk ones. The signal increased by powder indicates an easier magnetic field penetration into powdered superconductor and in this case the screening currents shade a relatively larger volume fraction, than in the case of bulk specimens.

In the following we try to explain our experimental results in the framework of a Josephson medium model supposing that the interstitial material or the grain boundaries, as weak links between the grains form a 3D network of percolative paths:

1) Since their linear dimensions are much bigger, than the grain sizes l [42], the effective junction length is limited only by the path's dimensions or particle's sizes.

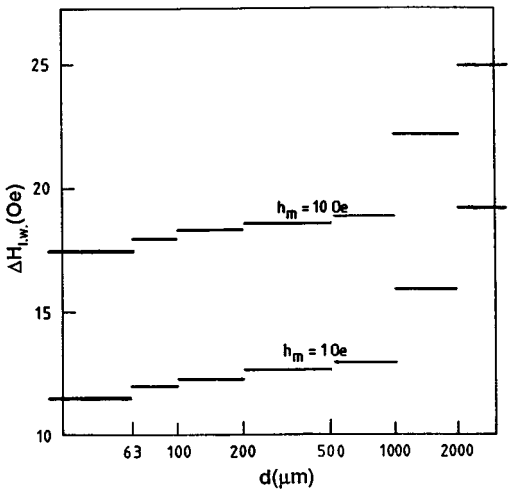

Fig. 16. The peak-to-peak line width of the field derivatives of microwave absorption signals depending on particle size ranges at modulation fields of 1 Oe and 10 Oe.

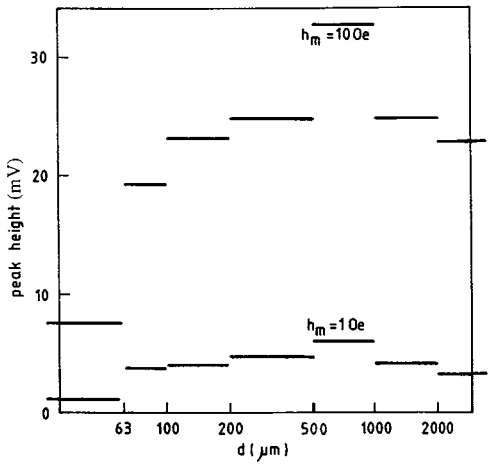

Fig. 17. The peak height distribution of the field derivative of microwave absorption on the particle size intervals at the modulation fields of 1 Oe and 10 Oe.

In this case the junctions can be characterized by their screening length, which is equal to Josephson penetration depth λ_J in order of 1 mm and the strongest screened field intensity [43] is characterized by

$$H_J = \frac{8\pi}{c}\lambda_J J_{Jc} = H_{ig} = H_{Jc}, \tag{7}$$

where J_{Jc} is the Josephson critical current density and H_J falls generally in the order of 0.1–1 Oe. The magnetic field dependence of microwave absorption of the Josephson junctions can be described in finite length approximation [44]. Presuming that the junctions of finite length may be associated with resonating cavities having characteristic dimensions equal to λ_J, the vortex penetration barriers completely disappear from the description and χ'' reaches a maximum value. This case is realized in the easiest way [45], when $d \approx \lambda_J$

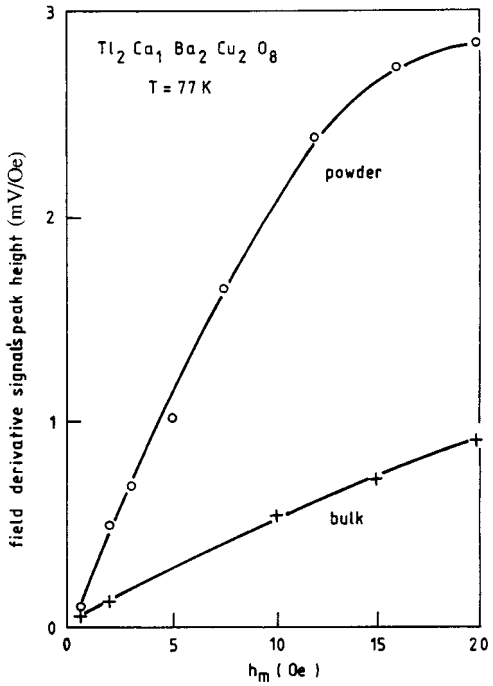

Fig. 18. The dependence of the peak height of the field derivative of microwave absorption on the modulation field intensity in bulk and powdered samples.

and then both the finite length theory and the cavity mode dissipation model motivate well the absorption maximum at this particle size.

2) Calculating $\lambda_J \approx 0.8$ mm from Figures 10, 15 and 16 and $H_{Jc} = 0.28\,\mathrm{Oe} = H_{ig}$ from Figure 13, the value of the critical current density for Josephson junctions can be obtained with the help of the relation (7), as $J_{Jc} = 2.2\,\mathrm{A/cm^2}$ at $T = 77$ K.
It is in the order of the magnitude provided by Ambegaokar Baratoff theory [46] for the grain-to-grain critical current density in the case of equivalent gaps and within the measured limits [47] got for other high-T_c superconducting samples.
3) The dependence of the Josephson critical magnetic field on the size of junctions can be determined by the expression [32]

$$H_{Jc} \approx \frac{\Phi_0}{2\lambda_L d_J}, \tag{8}$$

where Φ_0 is the flux quantum, λ_L is the London penetration depth and d_J is the junction's width. Since the typical value for λ_L of the present samples [37,48] is $\lambda_L = 0.12\,\mu$m, the variation of H_{Jc} is given as 0.17–0.08 Oe in the interval of $d_J = 0.5{-}1$ mm.
4) The trapped magnetic flux in the superconducting cavities causes a hysteretic shift of the absorption minimum, that can be described by the relation [44] of

$$\Delta H_{a.m.} \approx \pi e^{-l/\lambda_J} H_{Jc}. \tag{9}$$

In the case of $l = d = \lambda_J$ this formula gives a value for $\Delta H_{a.m.} = 0.33$ Oe. Measuring the secondary

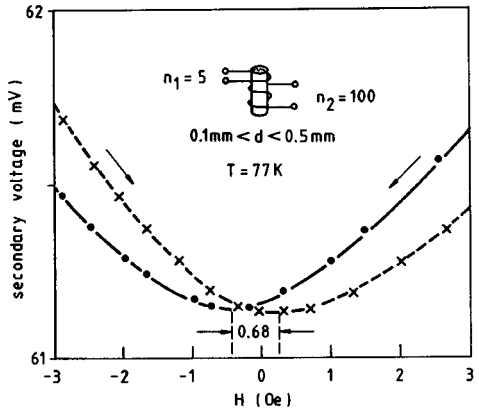

Fig. 19. Secondary voltage signal of a transformer, having crushed $Tl_2Ca_1Ba_2Cu_2O_8$ superconducting core of 0.1 mm $< d <$ 0.5 mm, which depends on the increasing and decreasing magnetic field. It represents a shift of the absorption minimum as $\Delta H_{\mathrm{a.m}} = 0.34$ Oe.

voltage signal of a transformer having superconducting ceramic $Tl_2Ca_1Ba_2Cu_2O_8$ core, the obtained $\Delta H_{\mathrm{a.m.}}$ shift of the minimum during the variation of the magnetic field has the value of $\Delta H_{\mathrm{a.m.}} = 0.34$ Oe (see Fig. 19), which supports the result obtained from (9).

5) Comparing our experimental data to other measured or calculated ones, a good correspondence between them can be verified. According to this, critical thickness of 0.22–0.44 mm for low vortex density in intermediate state in $Tl_2Ca_1Ba_2Cu_2O_8$ compounds [45] and $\lambda_{\mathrm{J}}(77\ \mathrm{K}) = 0.78$ mm, related to a 3D network of junctions [46] were determined and microwave noise anomaly produced by clusters of 0.4 mm size formed by interacting Josephson junctions was observed [32].

   On the basis of these similar results of different investigations, the sizes of percolative Josephson networks of 0.2–0.8 mm, containing numerous grains, can be supposed.

   Since the measured values of $H_{\mathrm{Jc}} = 0.28$ Oe, $\lambda_{\mathrm{J}} = 0.8$ mm and $J_{\mathrm{Jc}} = 2.2$ A/cm^2 are comparable to those referring to conventional, metallic, type II superconductors, it suggests that the intergranular coupling in sintered $Tl_2Ca_1Ba_2Cu_2O_8$ specimens can be treated as the network of metallic S–N–S weak links. It is supported by NMR investigation of this compound, too, which shows that the Tl-nuclei are in metallic state and environment [3].

6) At the same time, macroscopic particles having linear dimensions of about 1 mm may be taken into consideration as individual coherent domains, which are in superconducting or in normal state at a given time moment, depending on their microstructure and on the actual local temperature and magnetic field [36].

4 Conclusions

Based on the investigations of the dependence of a.c. susceptibility, r.f. susceptibility and microwave absorption on the temperature, magnetic field and on the particle size, the following conclusions can be drawn:

1) These investigations are suitable not only for qualitative characterization of the intergrain material of samples but to determine the actual values of the most important characteristic parameters, too, giving a reliable picture on their behavior in $Tl_2Ca_1Ba_2Cu_2O_8$ specimens, investigated. The magnitudes obtained by the measurements analyzed above are $\lambda_{\mathrm{J}} = 0.8$ mm for Josephson penetration depth, $H_{\mathrm{Jc}} = 0.28$ Oe for intergranular critical magnetic field and $J_{\mathrm{Jc}} = 2.2$ A/cm^2 for Josephson critical current density at $T = 77$ K.
2) The size effect of the main properties of this Tl-based compound has been directly detected for the superconducting volume fraction referring to 1% of every particle size interval, for the absorbed microwave energy and for line width and peak height of the field derivative of the absorption. Since all of these parameters distinguish the particle size of about 1 mm by a maximum or a sharp change, it can be explained as a critical value for the transition from the powder state to the bulk one, where coherent domains begin to develop in the specimens, responsible for the establishing macroscopic, global superconductivity.
3) It is demonstrated that the measurement of the dependence of r.f. susceptibility on the magnetic field provides information, which is equivalent to that obtained by the conventional experiments on a.c. susceptibility as the function of the temperature.
4) As is shown by using the shape of the size dependence of microwave absorption, the evolution of the experimental results according to the concept of a microwave induced cavity mode dissipation is equivalent to the finite size junction model to describe the intergrain material as a Josephson junction network. Since this concept is based directly on the measured data, it may lead to more precise results in certain cases, than the finite size junction model.
5) In order to control the characteristic data given by the direct measurement of the microwave absorption, the modulation technique seems to be an appropriate method. It can confirm the results of immediate absorption experiments providing values in coincidence to each other.

References

1. Z.Z. Sheng, A.M. Hermann, Nature **332**, 55, 138 (1988).
2. I. Kirschner, in *Studies of High Temperature Superconductors*, vol. 9, edited by A. Narlikar (New York: Nova Science Publ. Inc., 1992), pp. 149-192.
3. I. Kirschner, Gy. Kovács, I. Halász, R. Laiho, T. Porjesz, K. Tompa, T. Träger, T. Kármán, G. Zsolt, J. Less-Comm. Met. **150**, 229 (1989).
4. T. Nabatame, J. Sato, Y. Saito, K. Aihara, T. Kamo, S. Matsuda, Physica C **193**, 390 (1992).
5. W. Mexner, J. Hoffmann, S. Heede, K. Heinemann, H.C. Frayhardt, F. Ladenberger, E. Swarzmann, Z. Phys. B **101**, 181 (1996).

6. T. Kármán, E. Lähderanta, S. Leppävuori, I. Halász, I. Dódony, G. Zsolt, T. Porjesz, R. Laiho, A. Uusimäki, I. Kirschner, Gy. Kovács, Z. Phys. B **78**, 169 (1990).
7. E.V. Blinov, R. Laiho, E. Lähderanta, Y.P. Stepanov, K.B. Traito, Phys. Rev. B **51**, 3824 (1995).
8. M.A.R. Le Blanc, D.S.M. Cameron, S. Celebi, J.P. Pascal, Supercond. Sci. Technol. **11**, 359 (1998).
9. E.H. Harris, D.Z. Loftus, T.C.B. McLeish, P.Z. Ward, Supercond. Sci. Technol. **4**, 395 (1991).
10. I. Halász, V. Fülöp, I. Kirschner, T. Porjesz, J. Cryst. Growth **91**, 444 (1988).
11. I. Halász, A. Rockenbauer, I. Kirschner, T. Porjesz, J. Supercond. **1**, 451 (1988).
12. I. Halász, I. Kirschner, T. Porjesz, Gy. Kovács, T. Kármán, G. Zsolt, Cs. Sükösd, N. S.-Rozlosnik, J. Kürti, Physica C **153**, 379 (1988).
13. P.T. Wu, R.S. Liu, J.M. Liang, Y.T. Huang, L.J. Chen, Mod. Phys. Lett. B **3**, 15 (1989).
14. H. Kumakura, K. Togano, K. Takahashi, H. Simizu, M. Uehara, M. Maeda, M. Nakao, Jpn J. Appl. Phys. **27**, L857 (1988).
15. H. Iwasaki, N. Kobayashi, Y. Koiko, Y. Syono, K. Noto, Y. Muto, Jpn J. Appl. Phys. **27**, L1631 (1988).
16. B. Mühlschlegel, Z. Phys. **155**, 313 (1959).
17. R.A. Fischer, S. Kim, S.E. Lacy, N.E. Phillips, D.E. Morris, A.G. Markelz, J.Y.T. Wei, D.S. Ginley, Phys. Rev. B **38**, 11942 (1988).
18. V.L. Ginzburg, L.D. Landau, J. Exp. Teor. Fiz. **20**, 1064 (1950).
19. A.A. Abrikosov, J. Exp. Teor. Fiz. **32**, 1442 (1957).
20. L.P. Gorkov, J. Exp. Teor. Fiz. **36**, 1918 (1959); **37**, 833 (1959).
21. J. Bardeen, Phys. Rev. **105**, 554 (1954).
22. V.L. Ginzburg, J. Exp. Teor. Fiz. **30**, 539 (1956).
23. E. Helfand, N.R. Werthamer, P.C. Hohenberg, Phys. Rev. **147**, 295 (1966).
24. K.A. Müller, M. Takashige, J.G. Bednorz, Phys. Rev. Lett. **58**, 1143 (1887).
25. V. Calzone, M.R. Cimberle, C. Ferdeghini, M. Putti, A.S. Siri, Physica C **157**, 425 (1989).
26. H. Küpfer, S.M. Green, C. Hiang, Y. Mei, H.L. Luo, R. Meyer-Hirmer, C. Politis, Z. Phys. B **71**, 63 (1988).
27. P. Peyral, J. Rosenblatt, A. Rabotou, C. Lebeau, C. Perrin, O. Pena, A. Perrin, M. Sergent, Physica C **153**, 1493 (1988).
28. A. Gould, E.M. Jackson, K. Renouard, R. Crittenden, S.M. Bahgat, N.D. Spencer, L.E. Dohart, R.F. Wormsbecher, Physica C **156**, 555 (1988).
29. D.X. Chen, R.B. Goldfarb, J. Nogvés, K.V. Rao, J. Appl. Phys. **63**, 980 (1988).
30. G. Shaw, S.D. Murphy, S.Y. Li, A.-M. Stewart, S.M. Bhagat, IEEE Trans. Magn. **25**, 3512 (1989).
31. E. Simizu, D. Ito, Phys. Rev. B **39**, 2921 (1989).
32. J. Bohandy, B.F. Kim, F.J. Adrian, K. Moorjani, Phys. Rev. B **39**, 2733 (1989).
33. E.M. Jackson, G.J. Shaw, R. Crittenden, Z.Y. Li, A.M. Stewart, S.M. Bhagat, R.E. Glower, Supercond. Sci. Technol. **2**, 29 (1989).
34. E. Blinov, V.G. Fleisher, H. Huhtinen, R. Laiho, E. Lähderanta, P. Paturi, Yu.P. Stepanov, L. Vlasenko, Supercond. Sci. Technol. **10**, 818 (1997).
35. A.M. Portis, K.W. Blazey, K.A. Müller, J.G. Bednorz, Europhys. Lett. **5**, 467 (1988).
36. I. Kirschner, R. Laiho, A.C. Bódi, E. Lähderanta, Physica C **290**, 206 (1997).
37. I. Kirschner, S. Leppävuori, R. Laiho, A.D. Caplin, I. Halász, T. Porjesz, A. Uusimäki, G. Zsolt, E. Lähderanta, T. Kármán, J. Laverty, Gy. Kovács, Cryogenics **31**, 33 (1991).
38. I. Kirschner, I. Halász, Cs. Sükösd, T. Porjesz, J. Kürti, Gy. Kovács, L. Korecz, T. Kármán, N. S.-Rozlosnik, G. Zsolt, T. Träger, Phys. Lett. A **130**, 39 (1988).
39. M. Pojek, A. Dulŭic, B. Rakuin, Physica C **197**, 175 (1992).
40. B.L. Romakrishna, E.W. Ong, M.J. Igbal, J. Appl. Phys. **64**, 5803 (1988).
41. K.W. Blazey, A.M. Portis, Z.G. Bednorz, Solid State Commun. **65**, 1153 (1988).
42. S. Tyagi, M. Barsum, K.V. Rao, V. Skumryev, J.L. Costa, Physica C **156**, 73 (1988).
43. M. Tinkham, *Introduction to Superconductivity* (New York: McGraw-Hill Book Co, 1975).
44. A.D. Golubov, A.E. Koshalev, Physica C **159**, 337 (1989).
45. V.B. Geshkenbein, V.M. Vinokur, R. Fehrenbacher, Phys. Rev. B **43**, 3748 (1991).
46. V. Ambegaokar, A. Baratoff, Phys. Rev. Lett. **10**, 486 (1963).
47. H. Küpfer, I. Apfelstadt, R. Flükiger, C. Keller, R. Meier-Hirmer, R. Runtsch, A. Turowski, V. Weich, T. Wolf, Cryogenics **28**, 650 (1988).
48. I. Kirschner, S. Leppävuari, R. Laiho, A.D. Caplin, T. Kármán, E. Lähderanta, G. Zsolt, A. Uusimäki, J. Laverty, T. Porjesz, I. Halász, J. Levoska, Gy. Kovács, Z. Phys. B **78**, 381 (1990).